PHYSICAL REVIEW E, VOLUME 65, 061904

Metastable intermediates in the condensation of semiflexible polymers

B. Schnurr,[1,2,*] F. Gittes,[1,3,†] and F. C. MacKintosh[1,4,‡]
[1]*Department of Physics and Biophysics Research Division, University of Michigan, Ann Arbor, Michigan 48109-1120*
[2]*Department of Physics of Complex Systems, Weizmann Institute of Science, Rehovot 76100, Israel*
[3]*Department of Physics, Washington State University, Pullman, Washington 99164-2814*
[4]*Division of Physics and Astronomy, Vrije Universiteit, 1081 HV Amsterdam, The Netherlands*
(Received 14 December 2001; revised manuscript received 22 March 2002; published 14 June 2002)

Motivated by results from an earlier Brownian dynamics simulation for the collapse of a single, stiff polymer in a poor solvent [B. Schnurr, F. C. MacKintosh, and D. R. M. Williams, Europhys. Lett. **51**, 279 (2000)] we calculate the conformational energies of the intermediate (racquet) states suggested by the simulations. In the absence of thermal fluctuations (at zero temperature) the annealed shapes of these intermediates are well-defined in certain limits, with their major structural elements given by a particular case of Euler's elastica. In appropriate units, a diagram emerges that displays the relative stability of all states, tori, and racquets. We conclude that, in marked contrast to the collapse of flexible polymers, the condensation of semiflexible or stiff polymers generically proceeds via a cascade through metastable intermediates, the racquets, towards a ground state, the torus or ring, as seen in the dynamical simulations.

DOI: 10.1103/PhysRevE.65.061904 PACS number(s): 87.15.He, 36.20.Ey, 87.15.−v

I. INTRODUCTION

The conformation of individual polymer chains depends on the properties of their environment, i.e., the solvent [1–3]. In the presence of a *poor* solvent, isolated polymer chains tend to collapse toward compact states, in which polymer-solvent contacts are minimized. For flexible polymers, the kinetics of this coil-globule transition have been the subject of much research over the past few decades [4–9]. The kinetic pathway for flexible polymer collapse has only recently been experimentally confirmed to involve the formation of a pearl necklace and the gradual diffusion of large pearls from the chain ends [10,11].

In contrast to the flexible case, many polymers exhibit substantial bending stiffness, thus adding the (opposing) tendency to form extended structures. This makes a compact globule energetically unfavorable for *semiflexible* polymers because compact globules involve large amounts of bending. Such chains are described by the persistent or wormlike chain (WLC) model [3], examples of which include predominantly biopolymers (e.g., *F*-actin and DNA) but also some synthetic polymers (e.g., kevlar). The balance between the tendencies to straighten the filament (due to a bending energy) and to condense it (due to an effective short-range attraction or poor solvent) is at the heart of the condensation of semiflexible polymers.

The apparent equilibrium collapsed state for semiflexible polymers is well known: chains with significant bending stiffness can form rings or toroids to avoid incurring the large bending penalty of a spherical shell or a globule. This condensed state has been suggested and studied theoretically [12–15], demonstrated in a variety of experimental systems [16–21], and confirmed by computer simulation [22–25]. Theoretical work has predominantly addressed structural features, such as the detailed packing of filaments [26–31], while dynamical simulations and atomic force microscopy (AFM) among others have increasingly focused on kinetic aspects and condensation intermediates [19,20,24,32,33].

A particular set of recent dynamical simulations of isolated chains [34] has strongly suggested a possible (and in fact generic) pathway for the collapse of semiflexible polymers. These simulations showed not only the eventual formation of tori from extended chains quenched in poor solvent but demonstrated a series of long-lived, partially collapsed intermediate states. Very similar chain morphologies (our racquet states) also appear in other simulation work [24] and AFM studies of DNA condensation [19]. Motivated by these results, we develop and analyze a hierarchical family of metastable racquet states. In particular, we demonstrate that their relative conformational energies are consistent with the role they play in the simulations: they form an energetically driven cascade of increasingly compact conformations with sharp transitions between them.

We begin in Sec. II with a brief summary of the dynamical simulation results [34] that motivated this analysis. Section III addresses the morphology and evolution of the shapes to be analyzed in the remainder of the paper. Our approach to calculate the surface contributions to the conformational energies is developed in Sec. IV, followed by the two main sections containing a detailed analysis of torus and racquet states (Secs. V and VI, respectively). Section VII finally compares their relative stability and discusses the qualitative agreement with the dynamical simulation results we set out to understand.

II. BRIEF REVIEW OF THE DYNAMICAL SIMULATION RESULTS

The work described in Ref. [34] applied a standard Brownian dynamics (BD) algorithm [2] to a bead-and-spring model of a single polymer chain in the plane to capture the

*Electronic address: bernhard.schnurr@weizmann.ac.il
†Electronic address: gittes@wsu.edu
‡Electronic address: fcm@nat.vu.nl

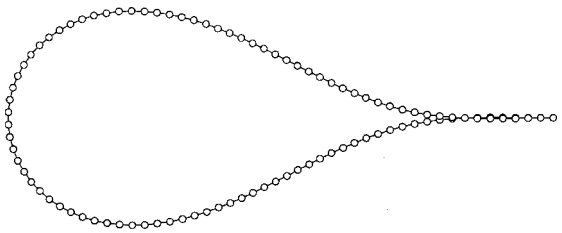

FIG. 1. Annealed shape of a racquet head from the BD simulation, achieved by slowly lowering the effective temperature once the structure has formed. The shape coincides with the analytical curve to within a linewidth.

most general features of a rather complex and biologically important process, the condensation of DNA. The technical details of that study are discussed elsewhere [34,35]. Here, we merely sketch the gross features and the generic results that motivated our work in this paper.

The dynamical evolution of a simulated chain followed a Langevin equation of the form

$$\xi \frac{dx_i}{dt} = -\frac{\partial U}{\partial x_i} + \eta_i(t) = F_{x_i} \tag{1}$$

for each bead i, where ξ is the coefficient of viscous drag ($\boldsymbol{F}_{\mathrm{visc}} = \xi \boldsymbol{v}$) and η the random noise. Each bead is displaced by $\Delta x_i = (F_{x_i}/\xi)\Delta t$ during a time step Δt. The potential U contains all interactions internal to the chain, including the bending energy, a short-range attractive interaction between beads (mimicking poor solvent conditions) and a very stiff longitudinal compliance. After thermalization of each chain, the solvent quality was quenched at $t = 0$.

Previous work [34,35] showed the typical dynamical evolution of a relatively short chain (a few persistence lengths) as a progression through well-defined stages identified by three types of conformations: extended chain with thermal undulations, various racquet states (see Figs. 1 and 2), and the torus or ring. We also pointed out that the end-to-end distance of the filament as a function of time changes sharply with the conformational transitions between states. It is important to note that the described conformations persist in time, as seen by quasiplateaus in the end-to-end distance evolution, each lasting for a considerable time of about 10^6 BD steps, about one-tenth of the entire condensation event. We can roughly estimate the correspondence between simulation steps and physical time for a particular system. To do this, we express the link length as a fraction of the persistence length and substitute for the local drag coefficient, assuming the viscosity to be of water. For *F*-actin, such an estimate suggests that an entire simulation of 10^7 BD steps models a filament for about 0.1 s. For DNA, this interval corresponds to a fraction of a millisecond.

Temporal persistence of racquet structures was seen throughout the simulations, suggesting that metastable intermediates are a general feature in this collapse. Presumably, energy barriers between intermediates are responsible for their local (meta)stability but we have not attempted to estimate their size.

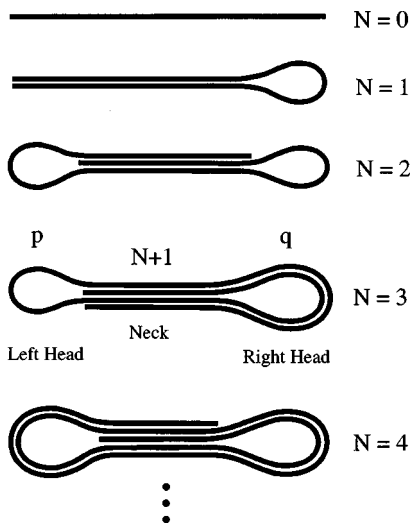

FIG. 2. Schematic ''family'' of racquet states. The rod can be thought of as a trivial racquet without a head ($N = 0$). All subsequent states are labeled by their number of head sections.

III. IDENTIFICATION OF INTERMEDIATE STATES

The dynamical simulations [34] suggest that the mechanism of collapse of semiflexible chains generically involves transitions through a series of long-lived intermediate states. In the absence of thermal fluctuations these intermediates anneal to certain underlying shapes that are well defined and allow a straightforward calculation of their conformational energies. The crucial element in the underlying shapes is a characteristic looped section that we call a racquet head. For the single racquet, the shape of the head (see Fig. 1) was produced in the simulation by annealing. While missing the effects of thermal undulations, our calculations of the conformational energies and detailed shapes of the annealed intermediates provide an insightful framework for understanding the simulation results.

In order to simplify the reference to specific states, we label all racquet states by their number of looped sections. Thus the rod is the $N = 0$ state, the racquet with a single loop at one end is the $N = 1$, and so forth, as indicated in Fig. 2. We refer to the loop formed at the ends of the structure as the ''head'' and to the bundle of filaments connecting heads as the ''neck.'' For the moment we neglect the more subtle question of the exact location of filament ends. Naively, one might assume that filament ends coincide with the ends of the neck, since it is straight; that is, the ends of the filament are expected to span the entire neck as they incur no bending penalty, but generally gain from increasing their overlap.

The picture as described provides an adequate starting point for labeling the states we consider here. Among the shapes indicated in Fig. 2 we distinguish two basic racquet symmetries: even and odd total numbers of heads *N*. For racquets with even *N*, the number of overlaps in the head sections is equal on the two sides, $p = q = N/2$. For racquets with odd *N*, one side (we arbitrarily call it the left, following Fig. 2) has one less $p = (N-1)/2$ than the other: $q = (N+1)/2$. As a consequence, the filament ends of an even racquet are on opposite sides of the neck.

FIG. 3. Early stages in the evolution of a long chain (300-mer, roughly $20\ell_p$) showing combinations of the conformational elements seen in shorter chains.

Note that the dynamical simulations modeled the case of fixed experimental conditions after the solvent quench. The polymer chain is merely exploring a given conformational energy landscape via thermal fluctuations. However, it can be instructive to consider as a *Gedankenexperiment* the case of variable filament length, and we use this perspective in our discussion. A (reduced) chain length is also a natural independent variable for the presentation and comparison of states. In this alternative perspective, the evolution of shapes starts with a short filament that gradually lengthens. At first, only the neck grows until the formation of a new head is favored. The incremental unit of growth between conformations thus consists of one head plus one neck segment. This procedure can be continued to arbitrary N, given enough filament. In Sec. IV C we will see that the appropriate formulation of the problem accomplishes changes in the (effective) filament length by adjusting the solvent quality instead of the actual chain length.

In the simulations, the actual transition into the torus state could not be resolved in detail. It is clear, however, that there are in principle at least two ways in which a loop can form: two chain segments can meet with their tangent angles at an angle of π or 2π. The former case leads to a racquet head, while the latter makes a ring that allows the chain to wind up into a torus directly. Since it is more likely for a stiff chain to bend into the smaller angle, one would expect the transition to racquets to be favored, at least for short chains. Statistically, the simulations [34] confirm this. Most of the chains studied there were relatively short (less than 10 persistence lengths) though a few examples (see Fig. 3) of longer chains showed qualitatively similar behavior but with increased complexity, such as the display of superstructures of racquets within racquets.

IV. CONFORMATIONAL ENERGIES

Having discussed the basic morphology of the intermediate states, we turn to the calculation of their conformational energies in the absence of thermal undulations. Racquet and torus conformations at zero temperature can be thought of as the underlying shapes, which become modified by fluctuations at finite temperatures. Apart from the bending contributions to the conformational energies, we need to describe the nature of the surface energy by which we model the poor solvent conditions that induce condensation. This surface energy assumes the packing or bundling of filaments in a hexagonal lattice (in cross section) and distinguishes between polymer and solvent exposures. The local arrangement into a hexagonal columnar phase has been confirmed, for example, by x-ray diffraction applied to bundles of DNA and other charged polymer chains [36–40] and the detailed structure within bundles of semiflexible polymer chains has been studied theoretically [41,42].

Our calculations describe the simplified model with filaments of vanishing thickness (compared to other length scales in the problem), while we model their packing on a perfect hexagonal lattice. Thus we do not take into account any winding defects due to topological constraints or variations in curvature due to the finite filament thickness. As implicit in the description of a wormlike chain, we assume a uniform bending modulus. In the torus state, such an ideal chain forms a circular ring with a single radius of curvature. Furthermore, we assume for both racquet heads and torus that partial filament overhang, an effective nonuniformity in the bending modulus, does not change their shape but only their size. Neglecting these higher order corrections is certainly justified in the limit that the bundling number N gets large.

A. Surface energy of hexagonal bundles

In a hexagonally close-packed bundle, each filament in cross section can be thought of as having six sites occupied by either solvent or polymer. The poor solvent lowers the energy for polymer-polymer relative to polymer-solvent contacts. To express the fact that there is a *relative* energetic advantage for filaments to bundle versus being exposed to solvent, we explicitly evaluate the total number of solvent-exposed sites and express the energy as a surface tension.

Particular surface energies are evaluated as follows. To find the coordination number α_N for an N bundle, consider the total number of surfaces or binding sites in the bundle with hexagonal order $(6N)$. This number is proportional to the energy of N individual filaments completely exposed to solvent. To account for the effect of bundling, we note that a bond corresponds to the merging of two binding sites on neighboring filaments. We thus subtract the number of bonds formed from only half the number of sites $(3N)$ to find the coordination number α_N. As an example of this numerology consider the cases for $N=5$ and 10: for five filaments there are seven bonds, resulting in a coordination of 8, while 10 filaments make 19 bonds and thus have a coordination of 11. Multiplying by the surface tension parameter γ finally yields the surface energy per unit length for such a bundle.

B. Filled shells and "magic" numbers

Differences between subsequent α_N's are always either 0 or 1 (except between $N=1$ and 2). This creates nonuniformities in the effective binding strengths per unit length, thus favoring particular bundling numbers. We expect this effect for N with the same coordination as their predecessor $(\alpha_N = \alpha_{N-1})$ but a coordination of one less than the $(N+1)$ bundle $(\alpha_N+1=\alpha_{N+1})$. This is the case whenever an added filament adds three instead of two bonds, thereby filling a shell. Examples of this situation are found for $N = 7,10,12,14,16,19,21, \ldots$ and we refer to them as magic numbers or filled shells. Cross sections of magic number

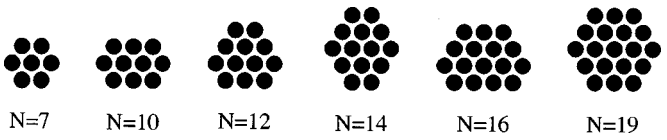

FIG. 4. Bundle cross sections of the lowest magic numbers on a hexagonal lattice. Note the arrangements of the "supermagic" numbers 7 and 19 into perfect hexagons.

bundles correspond to arrangements with high degrees of symmetry, as shown in Fig. 4.

A few supermagic numbers ($N=7,19,37,\ldots$) represent bundles with the special symmetry of the equilateral hexagon; we will not treat these cases separately. In agreement with Pereira and Williams [43] we find that bundles of magic numbers (and particularly the supermagic ones) play the role of preferred states with increased stability.

C. "Condensation" length and energy

The formulation of the problem as presented contains a characteristic length scale that greatly simplifies the discussion and presentation of our results. Balancing expressions for typical bending and surface energies ($\kappa/L \sim \gamma L$) for a given filament length L defines a measure that we call the *condensation length* $L_c \equiv \sqrt{\kappa/\gamma}$. Its role in the behavior of a chain under particular conditions is the following: given the physical parameters κ and γ, a filament much shorter than L_c will rarely self-intersect and therefore typically forms an extended structure, while one much longer than L_c is likely dominated by overlaps and will form collapsed or at least partially collapsed (intermediate) structures.

Another combination of the two basic parameters κ and γ sets an analogous energy scale, the *condensation energy* $U_c \equiv \sqrt{\kappa\gamma}$. With these measures, all conformational energies U_N can be presented in dimensionless units, where physical energies and lengths are normalized by their condensation values: $u_N \equiv U_N/U_c$ and $\lambda \equiv L/L_c$. This formulation also provides a convenient (experimental) realization of "changing the filament length." We can vary the reduced length λ by adjusting the values of κ and γ independently.

V. TORUS STATES

We describe a torus by the following two (dimensionless) variables: a filament of length λ is wound into a circle of constant radius ρ, as shown in Fig. 5. In general, the torus can have any number N of complete windings (through an angle 2π) and an amount of extra overhang σ subject to the condition $\sigma < 2\pi\rho$. Since the entire filament contour length λ has a constant curvature, the bending contribution to the conformational energy is always $\lambda/2\rho^2$.

We find it convenient to distinguish forms of the torus with different numbers of complete revolution N defined as the largest integer in $\lambda/2\pi\rho$. Any noninteger portion of this ratio represents overhang of filament beyond complete windings, defined as $\sigma \equiv \lambda - N(2\pi\rho)$. Our distinction of different tori by N naturally separates cases with different coordination numbers and thus different surface energies. In anticipation of an important distinction that emerges, we call a torus

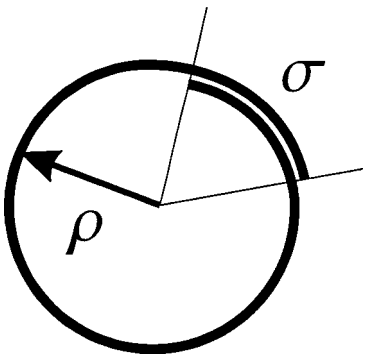

FIG. 5. Sketch of a generic torus (here a $1+$ in our labeling scheme) of radius ρ and overhang σ.

without extra overhang ($\sigma=0$) an "exact N" while we refer to the generic torus with finite overhang ($\sigma \neq 0$) as an "$N+$."

For the torus as described, we can then write down the following expression for its total conformational energy:

$$u_N^{\mathrm{torus}}(\lambda,\rho,\sigma) = \frac{\lambda}{2\rho^2} + 2\pi\rho[\alpha_N] + \sigma[\alpha_{N+1} - \alpha_N], \quad (2)$$

with the common bending term followed by two surface terms describing the contributions from the complete N-fold ring and the extra piece of overhang σ, respectively.

Substituting for σ leads to the torus energy in terms of λ and ρ only, which allows us to find the equilibrium size or radius $\rho_N(\lambda)$ for a particular state N by minimization with respect to ρ: note that $\partial^2 u_N^{\mathrm{torus}}/\partial\rho^2 = 3\lambda/\rho^4$ is positive everywhere. Resubstitution of $\rho_N(\lambda)$ yields the conformational energy $u_N^{\mathrm{torus}}(\lambda)$ in terms of the single variable λ. The expressions found in this way are valid in the ranges of λ between N and $N+1$ times the circumference $2\pi\rho_N$. However, a real solution for this equilibrium size need not exist. This happens exactly for the magic numbers with $N \geqslant 12$. When a real solution for the equilibrium radius does exist, the resulting energy has two terms: one proportional to $\lambda^{1/3}$, the other to λ. The coefficient of the linear term is the combination of coordination numbers ($\alpha_{N+1} - \alpha_N$) that can vanish for N just below the magic numbers (at $N = 6,9,11,13,\ldots$) leaving these cases with the functional dependence of $\lambda^{1/3}$ only. Another consequence of the numerology of hexagonal packing is that different states N can share the same energy expressions. Examples are the series $N=(2,3,4,5)$ and the pairs $N=(7,8),(17,18),(22,23),(25,26),(28,29),\ldots$. These cases form a particular class of transitions where σ grows continuously with λ.

A. Stability

The above method for finding the optimal torus sizes by minimizing the conformational energy represents the conventional approach to determine metastability. However, there is a somewhat unusual aspect to the problem at hand. The energy expressions for torus states with different N are

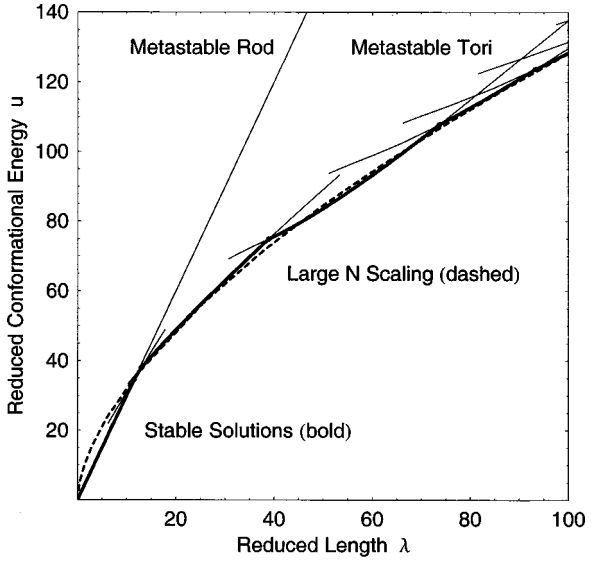

FIG. 6. Conformational energies of the torus states as a function of filament length in reduced units. The thinner lines indicate (metastable) solutions in regions where they are not the ground state, which in turn is indicated by bold segments. The dashed line shows the large N solution calculated in Sec. V C.

in general not the same. This introduces discontinuities in the form of the energy between adjacent states. Consequently, not only the conventional minima are identified by their vanishing slopes, but also another class of solutions is identified with discontinuities in slope at points where the energy expressions to the left and right differ due to the filament coordination. These are not minima in the usual sense (for instance, they are not locally quadratic minima); they are stabilized by finite slopes on both sides and do not have the usual signature of a vanishing slope. Our results for the tori are displayed in Fig. 6.

In order to establish the metastability of the tori of different N in more detail, we consider the behavior of the energy derivatives with respect to the radius $\partial u_N^{\mathrm{torus}}/\partial\rho$ evaluated at the radii where the exact N and $N+1$ form. These derivatives are all monotonic functions (functional dependence: $-\lambda^{-2}$) with at most a single zero indicating a limit of metastability. Around these zeros, the derivative is generically negative to the left and positive to the right. When negative, the energy is lowered by increasing the radius ρ, thus driving any overhang σ to vanish and making the torus an exact N. When positive, the opposite is true, driving σ to grow, making the torus an $N+$. Note that there are cases (notably again for the magic numbers with $N\geqslant 12$) where $\partial u_N/\partial\rho$ is negative everywhere. These cases form an important class in which tori never evolve (with increasing λ) towards states with finite overhangs: they remain metastable (with complete or exact overlap) for all lengths beyond some lower limit. The relative positions of the zeros in the energy derivatives combine in two fundamental ways, resulting in exact and $N+$ tori for various ranges of λ. A more detailed discussion of the various cases can be found in Ref. [35].

The rod ($N=0$) is of course a special (trivial) case without any bending contribution. Due to the absence of any competition between bending and self-affinity, the rod is (at least) metastable for all lengths and follows a straight line. The lower limit of the $1+$ state is given by the circumference of a single ring that just closes ($\lambda=2\pi$), a circle with the radius of a condensation length. The subsequent small N states show variations depending on the numerology of the hexagonal coordination numbers. For larger N a perhaps generic type of series emerges where $N+$ become exact $N+1$, which remain metastable to infinity. Thus, in contrast to what we have emphasized here by treating only cases with relatively small N in detail, only the few tori with N below 12 show variations to the generic pattern of exact (magic N) tori without extra overhangs.

TABLE I. Transition points for the lowest energy states (ground states) up to $N=24$. Only for the "shortest" chains (λ up to 11.543) is the rod stable to the torus.

State labels	Transition points
$0+\rightarrow 1+$	11.543
$1+\rightarrow 2+$	12.957
$2+\rightarrow 3+$	18.850
$3+\rightarrow 4+$	29.021
$4+\rightarrow 7$	38.871
$7\rightarrow 10$	73.625
$10\rightarrow 12$	93.195
$12\rightarrow 14$	119.876
$14\rightarrow 16$	148.687
$16\rightarrow 19$	155.672
$19\rightarrow 24$	228.700
⋮	⋮

A direct comparison between relevant branches of the solutions over regions of λ provides the transition points between stable (or ground) states, as summarized in Table I.

It appears that the majority of stable torus states (perhaps all $N\geqslant 12$) are exact states over their entire range. Their labels N are a subset of the magic numbers.

B. Discreteness

Another notable result are the discontinuities due to the hexagonal packing and the discrete coordination numbers. We might have expected the overhang σ and the torus size ρ to be continuous with changes in λ. At least for small N we find instead that small changes in λ can cause discrete jumps in the size of the ring ρ. This characteristic has previously been described by Pereira and Williams [43]. To what extent these effects are experimentally observable is not known. As N grows large, the effect should weaken and ultimately disappear altogether.

Discrete jumps are perhaps most prominently displayed as discontinuities in the torus size. Figure 7 shows the sizes or radii $\rho_N(\lambda)$ of the ground states as a function of λ. The first bold curve segment starts where the filament first makes a stable $1+$. Note that the functional dependence of the first two segments is different from the subsequent (linear) ones. The first two series evolve continuously according to their equilibrium solution for ρ_N with a functional dependence of

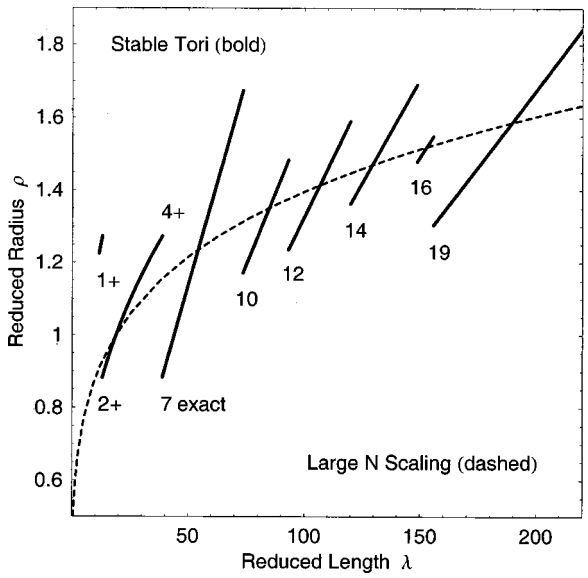

FIG. 7. Radii of the stable torus states (bold) as a function of filament length in reduced units, showing discrete transitions between the various series of states. The series shown are labeled by the states at their lower extremes. For comparison, the continuous large N solution is shown as a dashed line.

$\lambda^{1/3}$. Their prefactors are determined by some combination of the appropriate coordination numbers. By contrast, all subsequent segments are due to solutions that are constrained to be exact (by virtue of the magic numbers) and thus have the linear dependence of $\lambda/2\pi N$. The length of the various segments indicates the stability of the states they represent. Clearly, states with supermagic bundling numbers (the figure only shows $N=7$ and 19) are especially stable. The dashed line indicates the (continuous) solution found in the limit of large N, as discussed in the following section.

C. Large N limit and scaling

The scaling argument of the torus size with filament length goes back to the work of Ubbink and Odijk [28]. We sketch a similar argument here in order to compare it in Sec. VI D with the analogous argument for the racquets. First, we give the straightforward scaling argument. In a second pass, we then determine the prefactors based on the more accurate, hexagonally faceted cross section of the torus.

In the limit as N grows large, we can neglect such details as partial overhangs (finite σ) since differences between N and $N+1$ vanish as $1/N$. We assume first that the torus is a perfect cylinder with circular cross section. It grows as N, the number of filaments wound around its circumference. Thus, we expect the total torus surface area to scale as $\rho\sqrt{N}$. Substituting for the radius in a scaling sense ($\rho\sim\lambda/N$) we find that the conformational energy has two terms: one proportional to $\lambda/N^{1/2}$, the other to N^2/λ. Minimization with respect to N (implicitly letting N to be a continuous variable) yields the following set of scaling relations:

$$N\sim\lambda^{4/5}, \tag{3a}$$

$$\rho_\infty\sim\lambda^{1/5}, \tag{3b}$$

$$u_\infty\sim\lambda^{3/5}. \tag{3c}$$

To find the prefactors, we need to consider a geometrically more careful treatment. We assume that the torus formed has both a perfect hexagonal cross section and an integer winding number (no partial overhangs). These assumptions are reasonable: it can be shown by direct calculation that the surface tension for a fixed number of filaments on a triangular lattice is smaller for the hexagonal than for the circular cross section. This is analogous to a Wulff construction [44] that captures, for instance, the faceting of crystals in solid-state physics. The integer winding number is justified since the difference in the surface energies between N and $N+1$ filaments vanishes as N becomes very large.

For an (equilaterally) hexagonal cross section with its symmetries, we can determine the following relationships geometrically. As a characteristic for the size of the hexagon, we label the integer number of lattice spacings on a side by m. The counting of lattice sites (or filaments) in such a hexagonal bundle is $N=3m^2$ to leading order in m. Proper counting adds a linear and a constant term: $N=3m^2+3m+1$ but in the limit of large N we keep only the leading order in m.

We find the surface energy of such a bundle by counting solvent-exposed filament sites. A filament at an edge (of which there are $m-1$) exposes two sites, while one at a corner exposes three. Taking into account the sixfold symmetry of the hexagon, this results in $12m+6$ exposed sites on the surface. Substitution then yields the limiting coordination number (a surface energy per unit length) $\alpha_\infty=2\sqrt{3N}$ for a hexagonal bundle of N filaments. This coordination number also provides the prefactors for the conformational energy of the torus in the limit of large N,

$$u_\infty=\frac{2\sqrt{3}\lambda}{\sqrt{N}}+\frac{2\pi^2N^2}{\lambda}. \tag{4}$$

The expressions analogous to Eqs. (3) with geometrical prefactors are then

$$N=\frac{3^{1/5}}{(2\pi)^{4/5}}\lambda^{4/5}\approx 0.286\lambda^{4/5}, \tag{5a}$$

$$\rho_\infty=(6\pi)^{-1/5}\lambda^{1/5}\approx 0.556\lambda^{1/5}, \tag{5b}$$

$$u_\infty=\frac{5(3\pi)^{2/5}}{2^{3/5}}\lambda^{3/5}\approx 8.092\lambda^{3/5}. \tag{5c}$$

The last two expressions are shown in Figs. 6 and 7 as dashed lines. We see outstanding agreement between the large N limit and the exact solutions down to the lowest N in Fig. 6.

VI. RACQUET STATES

The racquet conformational energies are made up of bending contributions from each of the heads, and surface contributions from the heads as well as the neck region in

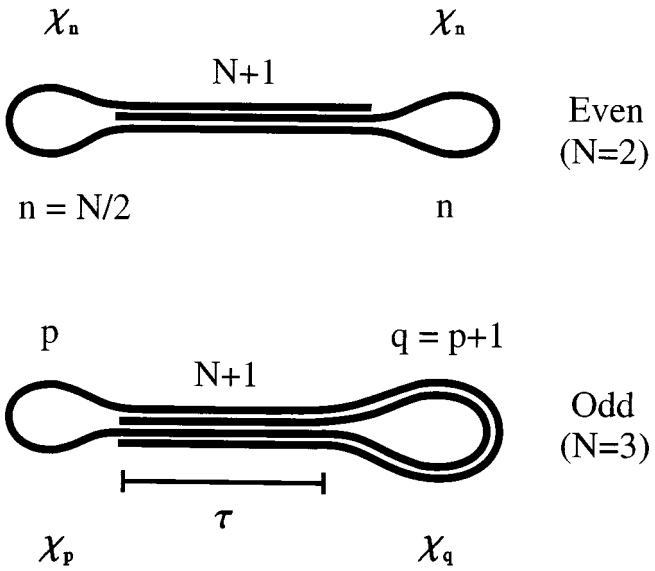

FIG. 8. Comparison of the structure and labels of generic even and odd racquets, represented here by the $N=2$ and 3. All the heads on one side are identical; the schematic separates head and neck filaments only to indicate their multiplicity.

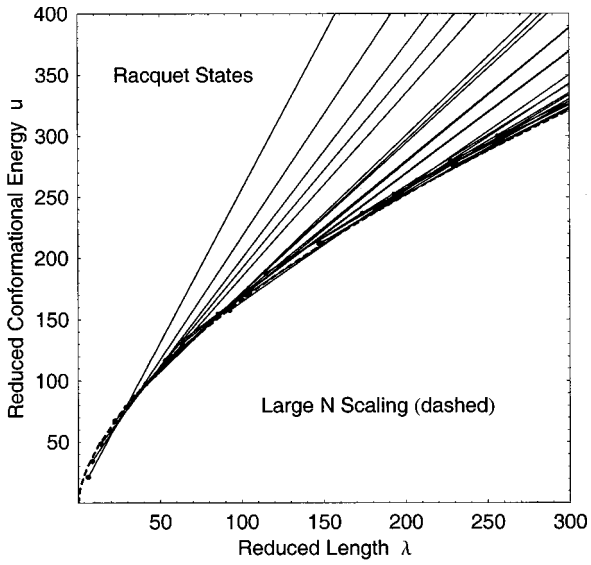

FIG. 9. Racquet state energies, shown as a function of filament length in dimensionless units, form a dense spectrum of solutions, each increasing linearly. For comparison, the scaling solution with proper prefactor in the limit of large N is superimposed (dashed line). Note the nearly perfect agreement of the scaling solution with the lower envelope of the racquet states, down to the very lowest values of N.

between. As shown in Fig. 8, the racquets divide naturally into two groups: those with even and odd numbers of heads.

In the even case, the number of heads on each side equals $n \equiv N/2$ by symmetry. In the odd case, we have $p \equiv (N-1)/2$ heads on the "left" and $q \equiv (N+1)/2$ on the "right." The labels left and right are our arbitrary naming convention (see Fig. 8). The variables p and q for the bundling numbers of the heads always differ by 1 ($q=p+1$) and sum to N. The bundling number of filaments forming the neck is always $N+1$.

Given these bundling numbers, the remaining variables (in dimensionless units) for the generic racquet are the overall filament length λ, and the head sizes on the two sides (namely, the contour lengths of the heads, labeled χ_p and χ_q). So far, we have described the racquets with their filament ends coinciding with the ends of the neck. However, in general (and in analogy with the overhang σ in the torus case) we need to allow for the extension of these ends into the heads, or the retraction into the neck. Lengths of overhang are labeled σ_p and σ_q and their sign indicates whether they extend into or retract back from the heads. The length of the neck τ is not an independent variable once all other parameters are fixed, since the total filament length imposes a constraint.

For the even racquet with a given λ, the number of variables reduces to only 2. Since the left and right heads for even racquets are identical by symmetry, we collapse their labels and are left with only one head size ($\chi_n \equiv \chi_p = \chi_q$) and a single overhang variable ($\sigma_n \equiv \sigma_p = \sigma_q$). The overall filament length for the even racquet is distributed into $\lambda_N^{\text{even}} = N\chi_n + 2\sigma_n + (N+1)\tau$ where the terms are ordered as heads, overhang, and neck. For the odd racquet, we leave the left and right head sizes separate, but require any overhang to be symmetrically distributed on the left side. This is not the only possible metastable solution, but the one we describe here generically is the most symmetrical; we will discuss the details of other possible solutions further in Sec. VI C. In the odd case, the overall chain length divides itself into $\lambda_N^{\text{odd}} = p\chi_p + q\chi_q + 2\sigma_p + (N+1)\tau$ where we use the single overhang variable σ_p to indicate that the two possible pieces of overhang are always on the left side (see Fig. 8).

By way of a preview, we state here that the racquet solutions (see Fig. 9) differ fundamentally from those of the tori. While the size of the torus was found to increase as a function of λ (up to discontinuities), the sizes of the racquet heads (as well as any lengths of overlap) are fixed for each state by the local force balance between the bundles of filaments making up head and neck. Having determined the head sizes and overhangs for a particular state, its lower limit of validity λ_{low} is found by adding up the head sizes and overhangs in the absence of any neck at all ($\tau \to 0$). This is the minimal filament length required to form a particular racquet. For all lengths beyond, the racquets remain metastable as their energies increase linearly with slope $\alpha_{N+1}/(N+1)$. Adding extra filament to any racquet configuration only lengthens its neck, while the head sizes and any overhang remain fixed. As a consequence, all racquets are (at least) metastable solutions for any λ beyond their lower cutoff λ_{low}. What remains to formulate the total conformational energies of the racquets is the bending contribution due to partial overhangs.

A. Head shape—an elastica

Having identified the racquet head as the distinguishing common element among the intermediate states, we calculate

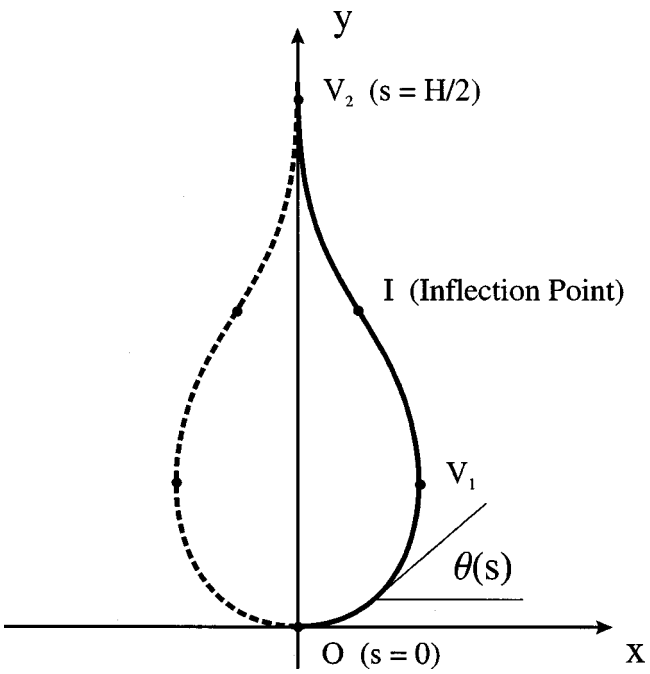

FIG. 10. Schematic figure of a racquet head with axes appropriate for our calculation. Local tangent angles θ are measured from the x axis. Symmetrical regions along the contour s are delimited by solid circles.

its geometrical shape (see Fig. 10) in the absence of thermal fluctuations from the bending of a slender, elastic rod. The expression for this head shape is necessary for the determination of bending energies for the racquets. The general class of shapes resulting from the bending of a slender rod by forces and couples applied at its ends only are known as *elastica*. Such solutions were first studied by Euler in 1744. The particular solution we seek is schematically drawn in Fig. 51 of the treatise by Love [45].

To solve for the shape of a racquet head of total contour length H we consider the geometry as shown and labeled in Fig. 10. In this section we use physical variables instead of the dimensionless units introduced previously, as they are more intuitive here and allow for dimensional analysis. Given the obvious symmetry about the y axis, it is sufficient to solve for one half of the racquet head only. The tangent angle along the curve increases from $\theta=0$ at the origin O ($s=0$), via a maximum at the inflection point I, to $\theta=\pi/2$ at V_2 ($s=H/2$, where the head joins the neck). Note that there are two points V_1 and V_2 at which the tangent is vertical ($\theta=\pi/2$), with an inflection point I between them. These three points define an additional symmetry (about the inflection point I) for the contour between points V_1 and V_2.

Our particular elastica is solved [46] by minimizing the WLC (wormlike chain) Hamiltonian subject to the boundary condition that the two halves of the head join in the neck at $x=0$. We impose this constraint by means of a Lagrange multiplier ζ,

$$U=\int_0^{H/2} ds\left\{\frac{\kappa}{2}\left(\frac{\partial\theta}{\partial s}\right)^2+\zeta\cos\theta\right\}. \tag{6}$$

Applying Euler's equation to this expression leads to the differential equation

$$\frac{d^2\theta}{ds^2}=-\beta^2\sin\theta(s), \tag{7}$$

where we made the substitution $\beta^2\equiv\zeta/\kappa$ and expressed the angle $\theta(s)$ explicitly as a function of the contour length s. Note that the Lagrange multiplier ζ has the dimensions of a force and expresses the force required to join the two filament bundles in the neck. Equation (7) can be integrated to yield an expression for the curvature along the head contour s as a function of the tangent angle θ,

$$\frac{d\theta}{ds}=\frac{2\beta}{k}\sqrt{1-k^2\sin^2(\theta/2)}. \tag{8}$$

Equivalently, one can rearrange terms and express the contour length s scaled by β in the form of an incomplete elliptic integral of the first kind $F(\phi,k)$,

$$\beta s=k\int_0^{\theta/2}\frac{dt}{\sqrt{1-k^2\sin^2(t)}}=kF(\theta/2,k), \tag{9}$$

where k is the elliptic modulus (yet to be determined) and t an integration variable. This is the parametric solution of an elastica: it gives the contour length s as a function of the tangent angle θ. The expression is multivalued over its range, but invertible in certain regions. Four such regions are defined by the axial symmetry of the head (through the origin and the neck) and the pair of inflection points in between. We thus cover the entire racquet head in a piecewise fashion, while only two of these regions are essentially different: the piece from O to V_1 and that from V_1 to I (with its reflection from I to V_2). The yet unknown elliptic modulus k for our elastica is found from a geometrical constraint. By the symmetry between the segments around the inflection point, we demand that the x value at point V_1 is twice that at the inflection point I. Solving the resulting equation numerically gives the value for the modulus as $k=1.1695$. The inflection point is identified by the vanishing curvature of Eq. (8), which corresponds to a tangent angle of $\theta_I=2.052$.

The expression for the curvature [in Eq. (8)] allows us to evaluate the bending energy of such a racquet head. Since the bending energy is an integral over the squared curvature, we can use Eq. (8) to evaluate this energy over any segment of the racquet head by integration. This requires the numerical evaluation of an incomplete elliptic integral of the second kind, $E(\phi,k)$,

$$U=\frac{\beta\kappa}{k}\int d\theta\sqrt{1-k^2\sin^2(\theta/2)}=\frac{2\beta\kappa}{k}E(\theta/2,k). \tag{10}$$

Adding up the symmetrical pieces of this solution for the entire head yields the total bending energy of a complete racquet head $U^{\text{head}}=A(\kappa/H)$ with A representing the numerical constant 18.3331. Thus, the bending energy in a racquet head depends (apart from the value for the bending modulus κ) only on its contour length. Note also that the

bending energy of the racquet head is very close to (but slightly below) that of a circular ring with the same contour length H ($U^{\mathrm{ring}}=2\pi^2\kappa/H\approx 19.7392\kappa/H$). Using circular rings as racquet heads would thus provide a reasonable approximation for the calculation of conformational energies, provided we neglect the penalty due to the sharp bends at the neck.

The form of the solution in Eq. (9) reveals that our racquet head shape or elastica is unique, in the sense that it is independent of any parameters in the problem. Both the parametric head shape $s(\theta)$ and the bending energy $U(\theta)$ are scaled by the factor β, related to the local force balance at V_2. The overall size of the resulting shape is merely scaled up or down, while its aspect ratio remains. Any slender, uniform rod, subject to these boundary conditions, will assume the described racquet head shape. We emphasize that the size of the racquet head does *not* depend on the overall filament length λ, unlike in the case of the torus.

This dependence of the head size on the local force balance also suggests that the following experiment should be possible, at least in principle. Evaluating head sizes in a sample of partially condensed filaments would measure the local interaction strength between filaments, a quantity not easily found by other means. This approach assumes of course, that the value for the bending modulus (or equivalently the persistence length) is known from an independent measurement.

B. Bending energy in racquet heads

To evaluate the bending contribution to the conformational energies we recall the expression for the bending energy in a head of size χ. Generalized to an N bundle (which effectively multiplies the bending modulus κ) the dimensionless bending energy for an N racquet head becomes $u_N^{\mathrm{head}}(\chi)=A(N/\chi)$, where A is again the same numerical constant evaluated previously from elliptic integrals. A stability analysis and numerical minimizations found that "perfect" racquets (with $\sigma=0$) are the solution for only a subset of all racquets.

In order to account for partial overhang into the heads, we need to generalize the notion of the numerical prefactor A. This "constant" is really a function of the partial overhang. Due to the scale invariance of our elastica, it is not surprising that A depends only on the *relative* overhang $\varsigma\equiv\sigma/\chi$. In terms of ς the four regions are delimited by the following values: 0, 0.1627, 0.5, 0.8373, and back to 1, measured from the neck. The three intermediate values identify the two inflection points and the halfway point (the origin in Fig. 10); note that these values are measured in the opposite sense from the one defined in the figure. Reconstruction of the piecewise solutions for any amount of partial overhang σ yields the expression $u^{\mathrm{partial}}(\sigma,\varsigma)=A(\varsigma)/\sigma$ with the numerical prefactor $A\equiv A(\varsigma=1)$ generalized to the *function* $A(\varsigma)$.

C. Even and odd racquets

The surface energy terms for all racquets consist of several terms with different coordination numbers in general. The only term the even and odd cases share is the coordination in the neck, whose length τ is shared by $(N+1)$ filaments. For the even racquet, symmetry simplifies the expressions somewhat. In each of its heads, we find a length $(\chi_n-\sigma_n)$ with coordination α_n and the overhang piece σ_n with coordination α_{n+1} while the neck has the common coordination α_{N+1}, which leads to the full expression for the conformational energy of the even racquet,

$$u_N^{\mathrm{even}}=A\left[\frac{N}{\chi_n}\right]+2A(\sigma_n/\chi_n)\left[\frac{1}{\sigma_n}\right]+2[\alpha_n(\chi_n-\sigma_n)+\alpha_{n+1}(\sigma_n)]+\alpha_{N+1}(\tau). \tag{11}$$

The first two terms are the bending contributions for complete heads and partial overhang, while the three following terms are surface contributions for head segments and neck, respectively. For the odd racquets, the expression becomes

$$u_N^{\mathrm{odd}}=A\left[\frac{p}{\chi_p}+\frac{q}{\chi_q}\right]+2A(\sigma_p/\chi_p)\left[\frac{1}{\sigma_p}\right]+\alpha_p(\chi_p-2\sigma_p)+\alpha_q(\chi_q+2\sigma_q)+\alpha_{N+1}(\tau). \tag{12}$$

In the even case, there are only two free variables, χ_n and σ_n. We find their optimal values by simultaneous, numerical minimization. In the odd case, the situation is slightly different, since we lack the symmetry between heads. However, we can make use of the fact that both filament ends (and therefore any potential overhang σ) are on the left side. This leaves the right head with a well-defined structure of q filaments in the head and $N+1=2q$ filaments in the neck. Since the head size is solely determined by the respective bundling numbers in head and neck, we can determine right head sizes independently of any overhang on the left by minimization in terms of the various bundling and coordination numbers and A only,

$$\chi_q=\sqrt{\frac{2qA}{2\alpha_q-\alpha_{2q}}}. \tag{13}$$

We then numerically minimize over the two remaining free variables χ_p and σ_p of the left head. Plotting constant energy contours as a function of the two free variables generally reveals the approximate location of the relevant minimum, and their coordinates were used as a starting point for the minimization routine. This procedure finds two possible outcomes for both even and odd cases. In the simpler case, the energy is minimized without overhang ($\sigma=0$) and we recover the naively assumed, perfect racquet structure. In the other case, we find a local minimum with respect to σ and χ for finite values of overhang. In every case we have checked (up to $N=30$), these solutions put the fractional overhang in the second region of the racquet head, between the inflection and halfway points, as indicated in Fig. 11.

Since both filament ends are on the same (left) side for the odd racquets, there are several possible configurations for overhang to be arranged, as shown in Fig. 12. The two pieces of equal length σ_p could be arranged symmetrically on opposite sides of the head. Alternatively, the two pieces of overhang can be on the same side, but not necessarily of

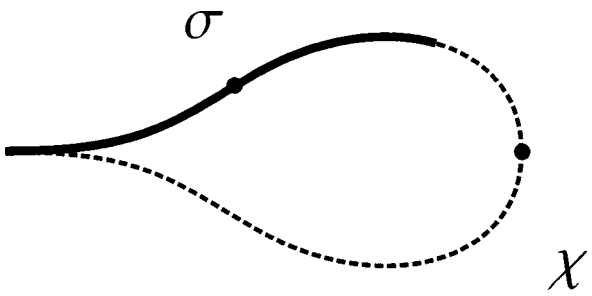

FIG. 11. Partial overhang σ (solid line) into an existing head of size χ (dashed). The ratio of σ/χ defines the fractional overhang ς. This schematic shows the typical situation for racquet solutions with nonzero overhang, with the filament end located somewhere between the inflection and the halfway points (solid circles).

equal length. All the cases we examined are minimized for one unique value of σ, corresponding to cases (a) and (c) in Fig. 12, which turn out to be degenerate in energy. In retrospect we were thus justified to describe the odd racquet with overhang generically as the symmetric case (a), while a second (asymmetrical) solution, degenerate in overhang and energy, exists.

All racquet head sizes χ_p and χ_q found either by direct calculation or by numerical minimization are displayed as a function of the racquet state label N in Fig. 13 to show the general trend and their convergence towards the large N solution. Head sizes typically increase with N, though not monotonically, and right heads are typically larger than left for the odd racquets. Even racquet heads are of the same size, by construction.

Since our minimization allowed only for extension into the heads but not retraction of the filament ends back into the neck, we tested the stability of racquets (up to $N=30$) to small perturbations, subject to fixed overall length λ. We found three types of results. In the simplest case, the racquets are stable to any small change. These racquets (with $N=1,2,3,11,15,17,20,\ldots$) remain exact ($\sigma=0$). A second class is identified by stability to retraction but not to extension. These racquets (with $N=4-10,13,18,22,\ldots$) develop finite (positive) overhang. The remaining cases are the magic numbers starting with 12 (namely, $N=12,14,16,19,21,\ldots$), which are unstable (or marginally stable) to retraction along the neck. A subset of these states are unstable to extension, and solutions with finite, positive overhang exist. However,

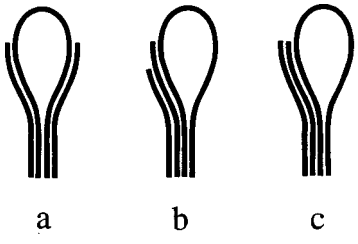

FIG. 12. Three possible solutions for partial overhang into the left head of an odd racquet. Case (a) is the one described in the text. The more general case with different amounts of overhang on the same side (b) is always minimized by the arrangement in case (c) where the two ends coincide.

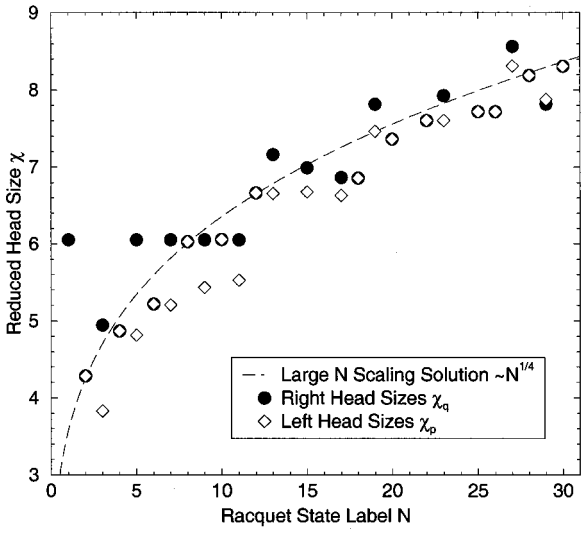

FIG. 13. Left and right head sizes versus the state label N. Pairs of even heads are of the same size, by symmetry. The general trend is for heads to grow with N, if not monotonically. Notice the convergence towards the asymptotic solution [dashed line, see Eqs. (14)] with increasing N.

those cases that are stable to extension have no metastable solution at all. We thus conclude that no racquet solutions exist for $N=14,16,21,24,\ldots$ and these states are omitted from our energy spectra (Fig. 9) and the series of head sizes (Fig. 13).

D. Large N limit and scaling

We perform the analogous calculation to that done for the torus states in Sec. V C, under the assumption that bundles form hexagonal cross sections as their bundling numbers N become large, to find the behavior of the racquet energies in the same limit. The result is shown as the dashed lines in Figs. 9 and 13. To compute it, we assume that the large N racquet be even and without overhang ($\sigma=0$) as differences between bundles of nearly the same number of filaments vanish in this limit. This even racquet has a neck length τ and a limiting head size χ_∞ for large bundling numbers n in the heads and N in the neck (see Fig. 14).

Since the size of the heads depends only on the balance of forces at the point where the head and neck bundles meet, we can calculate the optimal head size χ_∞ as in Eq. (13) for the right head of an odd racquet. As in Sec. V C, we determine the optimal bundling number $N_{\rm opt}(\lambda)$ by minimizing the energy with respect to N, which yields the scaling results with prefactors as functions of λ only,

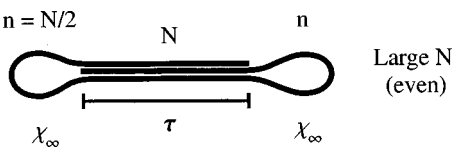

FIG. 14. Schematic racquet in the limit of large N where we assume the symmetry of the even racquet and neglect any extra overhang.

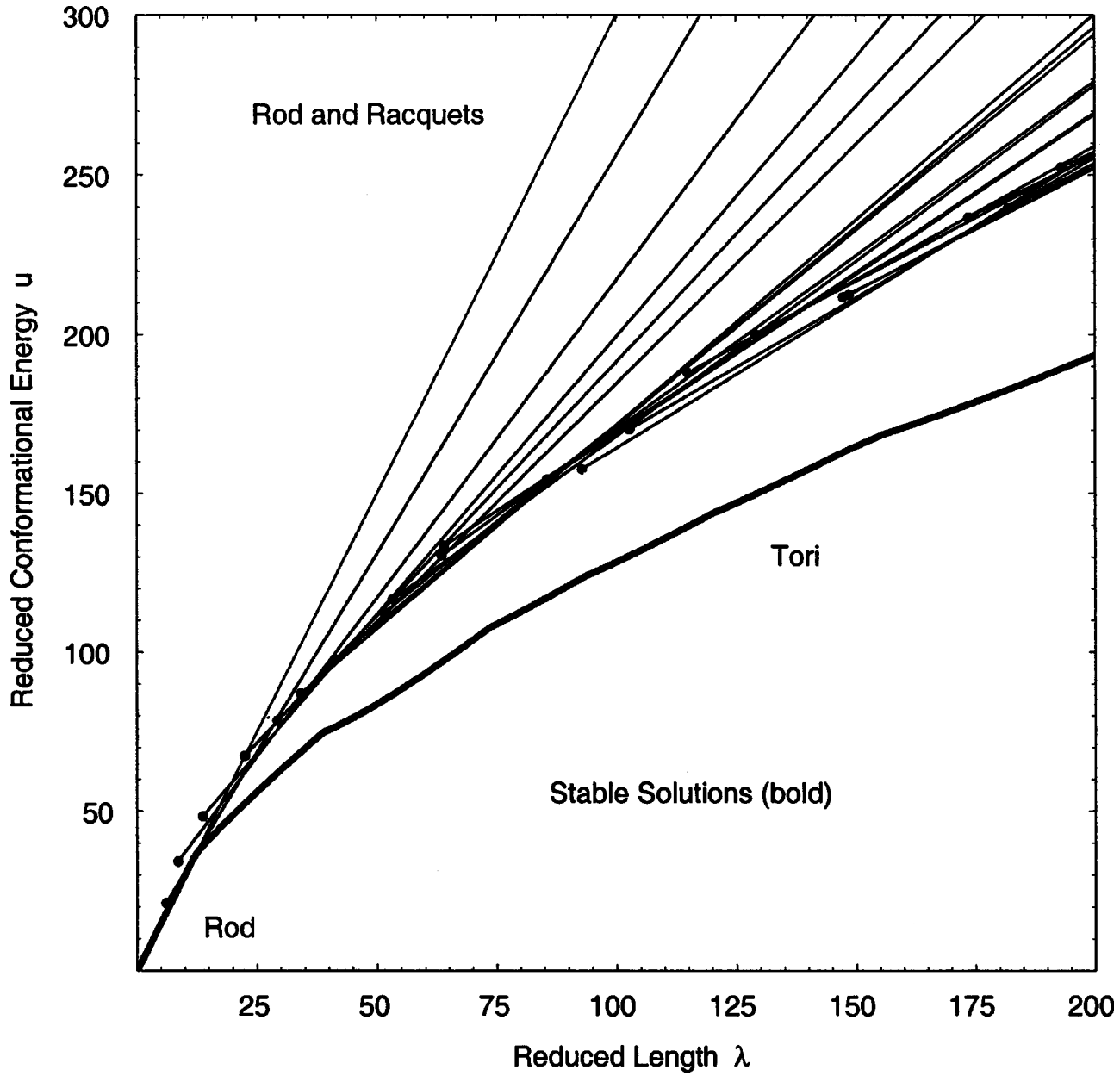

FIG. 15. Spectrum of rod, racquet, and torus states shown as conformational energy versus filament length in reduced units. Only the rod (at small λ) and the tori (for all λ beyond a transition point) are globally stable states. Notice the rather large gap between the spectrum of racquet states and the stable torus solution. Metastable torus solutions are omitted for clarity.

$$N_{\mathrm{opt}} \approx 0.303\lambda^{4/5}, \tag{14a}$$

$$\chi_{\infty} \approx 2.653\lambda^{1/5}, \tag{14b}$$

$$u_{\infty} \approx 10.482\lambda^{3/5}. \tag{14c}$$

Knowing the head size χ_{∞}, we can calculate the lower limit of validity λ_{low} in a scaling sense. This allows us to compare the expressions for the filament length from minimization ($\lambda_{\mathrm{opt}} \approx 4.442N^{5/4}$) with the length found by simply removing the neck altogether ($\lambda_{\mathrm{low}} \approx 3.575N^{5/4}$). Since the optimal length λ_{opt} exceeds the minimal length λ_{low}, a large N racquet will be one with a finite neck. This is an important result since it hints at the evolution of very long chains as they condense into racquets with increasingly larger N. In fact, we can estimate the growth of the neck length τ_{∞} from the difference between the prefactors in λ_{low} and λ_{opt}. Its scaling is given by $\tau_{\infty} \approx 0.644\lambda^{1/5}$. Thus, the neck grows with the same power of λ as the heads but with a smaller prefactor. We may have anticipated that the growing heads provide a simple pathway towards the torus, as the inevitable limit of the heads growing at the expense of the neck. For a fixed filament length, the neck would have had to shrink to zero with increasing N, opening up the structure to form a torus.

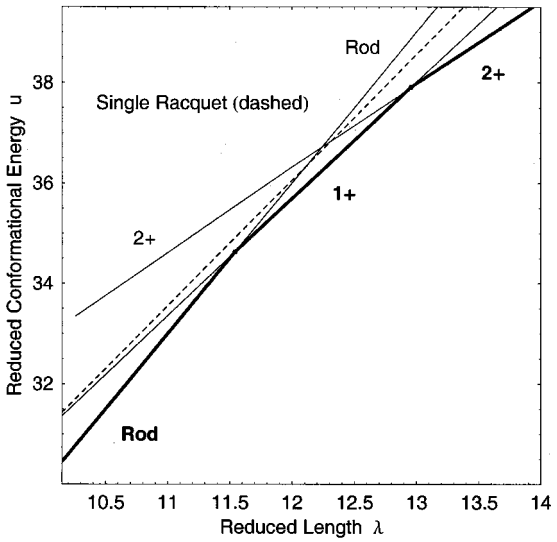

FIG. 16. Close-up of the rod, racquet, and torus solutions in the region where they are closest to each other. Racquets are indeed never stable, though their energy is very close to both the rod and the tori in this region.

For the particular racquet solutions shown in Fig. 9 we notice that the end points are relatively dense and represent, at times, the lowest point in the spectrum of states. Especially for such states, it is still true that their neck can shrink to very small or vanishing lengths, depending on λ. Thermal fluctuations can then lead to the opening up of the neck to form a torus. Yet, even if the limit of large N does not provide an absolutely compelling pathway for the collapse to the torus, we now appreciate the energetics involved.

VII. DISCUSSION: RACQUETS VERSUS TORI

Figure 15 shows the individual racquet solutions of Fig. 9 now compared to the stable torus ground states found in Sec. V A. In anticipation of these results, we described the lowest metastable torus state over any range of λ as the ground state of the system. Figure 15 confirms this claim by direct comparison of racquets and tori. In addition, we found that the large N solutions for tori and racquets both grow as $\lambda^{3/5}$ but with different prefactors. In combination with the close agreement between particular solutions and the large N limit, this strongly suggests that the torus remains in the ground state for all λ beyond the transition point ($\lambda = 11.543$). Only for shorter chains, does the rod represent the ground state.

There appears to be only one region where the energies of racquets and tori are even close, at the very low values of λ near the transition point. Figure 16 shows the relevant region in detail. The $N=1$ racquet solution comes extremely close to the solutions for both the rod ($N=0$) as well as the 1+ torus, but remains above. Thus the only stable (ground state) solutions for this system (in the absence of thermal fluctuations) are the rod at small λ and the tori everywhere beyond the transition point. At energies above this ground state, we see a dense spectrum of metastable solutions, made up of other (metastable) torus (see Fig. 6 for details) and increasing number of racquet states.

For fixed conditions we need only consider a vertical slice through the spectrum of energies. Along such a line, we can imagine a filament cascading down from an extended, rodlike configuration, through various metastable intermediates, while lowering its energy along the way. Our calculations do not of course capture the entire physical picture, as we neglect filament size in the bundling and our states are calculated in the absence of thermal undulations. So far we have no estimate of the energy barriers between the metastable intermediates. However, the dynamical simulation results [34] suggest that these barriers as well as the energy gaps between states are large compared to k_BT: transitions that increase N are infrequent and sharp, while transitions in the opposite direction are essentially never observed. This is especially true for the transition from the racquet spectrum to a torus, indicating that this energy gap is even larger for the parameters chosen in the simulation. This picture is consistent with the analytic results in Fig. 15 that clearly shows the large gap stabilizing the ground state. The results of our analysis thus nicely corroborate, at least qualitatively, the results of our prior computer simulations as well as their relevance to the condensation of stiff chains.

We would like to note that the shape of condensed filaments may depend on the nature and molecular structure of the condensing agent. Our study only addresses an interaction that is uniform along the filament, such as the effect due to a poor solvent. Other systems, with more pointlike organizing centers, have been shown to exhibit intricate multileaf or flower patterns [32,47].

Our observations suggest that the pathway for the collapse of extended chains into condensed structures via intermediate racquet states is a viable, even generic alternative to the perhaps more immediately guessed direct winding up upon the meeting of filament ends at an obtuse angle. Some of the simulations show the latter collapse pathway, but it is much less frequent. Furthermore, this cascade picture through which our calculations reinforce and at least partially explain the simulation results, seems robust. We find this cascade through intermediate states even for a much more naive treatment of the poor solvent interaction used in a first pass. The individual curves (e.g., in Fig. 15) are shifted but show a qualitatively similar picture. The generic cascade through metastable intermediates is so dominant that it is retained regardless of the detailed realization of the interactions.

ACKNOWLEDGMENTS

The authors wish to thank David Williams for helpful discussions, including sharing aspects of related work [43]. This work was supported in part by the Whitaker Foundation and by NSF Grant Nos. DMR-9257544 and INT-9605179. B.S. acknowledges support from the Minerva Foundation (Max Planck Society).

[1] P.-G. deGennes, *Scaling Concepts in Polymer Physics* (Cornell University Press, Ithaca, 1979).
[2] M. Doi and S.F. Edwards, *The Theory of Polymer Dynamics* (Clarendon Press, Oxford, 1988).
[3] A.Y. Grosberg and A.R. Khokhlov, *Statistical Physics of Macromolecules*, AIP Series in Polymers and Complex Materials (AIP Press, New York, 1994).
[4] P.G. deGennes, J. Phys. (France) Lett. **46**, L639 (1985).
[5] B. Ostrovsky and Y. Bsar-Yam, Europhys. Lett. **25**, 409 (1994).
[6] A. Buguin, F. Brochard-Wyart, and P.G. deGennes, C. R. Seances Acad. Sci., Ser. 2 **322**, 741 (1996).
[7] K.A. Dawson, E.G. Timoshenko, and Y.A. Kuznetsov, Physica A **236**, 58 (1997).
[8] A. Halperin and P.M. Goldbart, Phys. Rev. E **61**, 565 (2000).
[9] N. Lee and D. Thirumalai, Macromolecules **34**, 3446 (2001).
[10] B. Chu, Q.C. Ying, and A.Y. Grosberg, Macromolecules **28**, 180 (1995).
[11] C.F. Abrams, N. Lee, and S. Obukhov, e-print cond-mat/0110491 2001 (unpublished).
[12] A.Y. Grosberg, Biofizika **24**, 32 (1979).
[13] V.A. Bloomfield, Biopolymers **31**, 1471 (1991).
[14] V.A. Bloomfield, Biopolymers **44**, 269 (1997).
[15] V.V. Vasilevskaya, A.R. Khokhlov, S. Kidoaki, and K. Yoshikawa, Biopolymers **41**, 51 (1997).
[16] A.Z. Li, T.Y. Fan, and M. Ding, Sci. China, Ser. B: Chem., Life Sci., Earth Sci. **35**, 169 (1992).
[17] Y. Fang and J.H. Hoh, Nucleic Acids Res. **26**, 588 (1998).
[18] M.R. Shen, K.H. Downing, R. Balhorn, and N.V. Hud, J. Am. Chem. Soc. **122**, 4833 (2000).
[19] A.L. Martin, M.C. Davies, B.J. Rackstraw, C.J. Roberts, S. Stolnik, S.J.B. Tendler, and P.M. Williams, FEBS Lett. **480**, 106 (2000).
[20] D. Liu, C. Wang, Z. Lin, J.W. Li, B. Xu, Z.Q. Wei, Z.G. Wang, and C.L. Bai, Surf. Interface Anal. **32**, 15 (2001).
[21] H.G. Hansma, Annu. Rev. Phys. Chem. **52**, 71 (2001).
[22] H. Noguchi, S. Saito, S. Kidoaki, and K. Yoshikawa, Chem. Phys. Lett. **261**, 527 (1996).
[23] A. Byrne, E.G. Timoshenko, and K.A. Dawson, Nuovo Cimento Soc. Ital. Fis., D **20**, 2289 (1998).
[24] H. Noguchi and K. Yoshikawa, J. Chem. Phys. **113**, 854 (2000).
[25] M.J. Stevens, Biophys. J. **80**, 130 (2001).
[26] N.V. Hud, Biophys. J. **69**, 1355 (1995).
[27] N.V. Hud, K.H. Downing, and R. Balhorn, Proc. Natl. Acad. Sci. U.S.A. **92**, 3581 (1995).
[28] J. Ubbink and T. Odijk, Biophys. J. **68**, 54 (1995).
[29] J. Ubbink and T. Odijk, Europhys. Lett. **33**, 353 (1996).
[30] S.Y. Park, D. Harries, and W.M. Gelbart, Biophys. J. **75**, 714 (1998).
[31] V.L. Golo, E.I. Kats, and Y.M. Yevdokimov, J. Biomol. Struct. Dyn. **15**, 757 (1998).
[32] Y. Fang and J.H. Hoh, J. Am. Chem. Soc. **120**, 8903 (1998).
[33] S.Q. He, P.G. Arscott, and V.A. Bloomfield, Biopolymers **53**, 329 (2000).
[34] B. Schnurr, F.C. MacKintosh, and D.R.M. Williams, Europhys. Lett. **51**, 279 (2000).
[35] B. Schnurr, Ph.D. thesis, University of Michigan, 2000.
[36] Y.M. Evdokimov, A.L. Platonov, Y.M. Varshavsky, and A.S. Tikhonenko, FEBS Lett. **23**, 180 (1972).
[37] T. Maniatis, J.H. Venable, and L.S. Lerman, J. Mol. Biol. **84**, 37 (1974).
[38] Y.M. Evdokimov, T.L. Pyatigorskaya, O.F. Polyvtsev, N.M. Akimenko, V.A. Kadykov, D.Y. Tsvankin, and Y.M. Varshavsky, Nucleic Acids Res. **3**, 2353 (1976).
[39] R. Podgornik, D.C. Rau, and V.A. Parsegian, Macromolecules **22**, 1780 (1989).
[40] R. Podgornik and V.A. Parsegian, Macromolecules **23**, 2265 (1990).
[41] T. Odijk, Biophys. Chem. **46**, 69 (1993).
[42] T. Odijk, Europhys. Lett. **24**, 177 (1993).
[43] G.G. Pereira and D.R.M. Williams, Europhys. Lett. **50**, 559 (2000).
[44] G. Wulff, Z. Kristallogr. **34**, 449 (1901).
[45] A.E.H. Love, *A Treatise on the Mathematical Theory of Elasticity* (Dover, New York, 1944).
[46] F. Gittes, Ph.D. thesis, University of Washington, 1994.
[47] H. Schiessel, J. Rudnick, R. Bruinsma, and W.M. Gelbart, Europhys. Lett. **51**, 237 (2000).